J. Fluid Mech. (1986), *vol.* 171, *pp.* 71–100
Printed in Great Britain

A linear stability theory of double-diffusive horizontal intrusions in a temperature–salinity front

By HIROSHI NIINO

Meteorological Research Institute, 1-1, Nagamine, Yatabe, Tsukuba, Ibaraki 305, Japan

(Received 18 October 1984 and in revised form 13 March 1986)

The stability of a temperature–salinity front of finite width in which the density is exactly compensated for in the horizontal direction is studied by means of a linear theory. It is assumed that salt fingers are responsible for vertical transports of salinity and heat. The front is found to be always unstable even if viscosity is present. Horizontal intrusions are generated as a result of the instability, and cold/fresh water sinks while hot/salty water rises.

The stability of the front is described by three dimensionless parameters: a frontal stability parameter $G = [g(1-\gamma)\beta\Delta S]^6/\kappa_e^2 a^2 N^{10}$, a stratification parameter $\mu = g(1-\gamma)\beta\overline{S_z}/N^2$ and a Schmidt number $\epsilon = \nu/\kappa_e$, where g is the acceleration due to gravity, β the salinity contraction coefficient, ΔS half of the salinity difference across the front, γ the density-flux ratio of temperature to salt due to salt fingers, N the Brunt–Väisälä frequency corresponding to the basic density stratification, a the half-width of the front, $\overline{S_z}$ the vertical gradient of the basic salinity, κ_e the eddy diffusivity of salt due to salt fingers, and ν is either molecular or eddy kinematic viscosity. When ϵ is not zero it is found that a modified frontal stability parameter R defined by $R = G/\epsilon$ plays an important role in determining the stability for a fixed value of μ. In particular, when ϵ is larger than 10, the stability is almost completely determined by R if μ is specified.

The dependence of the vertical scale h of the fastest-growing mode on external parameters varies according to the value of R for a given value of μ. When R is less than $40(1+\mu)^{5.4}$ (for $\epsilon = 10^{-3}$–10^3) h becomes independent of R and ϵ and is given by $h = 2.2d/(1+\mu)$, where $d = g(1-\gamma)\beta\Delta S/N^2$ is the scale suggested by Ruddick & Turner (1979) who performed an experiment on horizontal intrusions across a narrow front. When $R > 2\times 10^5(1+\mu)^{4.9}$, on the other hand, h becomes proportional to $dR^{-\frac{1}{4}}$, the scale suggested by Toole & Georgi (1978), who considered the stability of a temperature–salinity front of infinite width. The constant of the proportionality is a weak function of ϵ and varies from $2\pi[(2+\mu)/4(1+\mu)^2]^{-\frac{1}{4}}$ to $2\pi[2(1+\mu+(1+\mu)^{\frac{1}{2}})]^{\frac{1}{2}}$ as ϵ goes from zero to infinity. Thus a front can be said to be narrow if $R < 40(1+\mu)^{5.4}$ and wide if $R > 2\times 10^5(1+\mu)^{4.9}$.

The results of the theory explain those of Ruddick & Turner's experiment (1979) reasonably well.

1. Introduction

One common characteristic of oceans is that interleaving layers are found where there are strong gradients of temperature and salinity in the horizontal direction. The possibility of a cooperative instability in which salt fingers drive medium-scale

intrusions, which in turn provide a necessary amount of salt flux to maintain salt fingers, has been suggested theoretically by Stern (1967). Recent observations in oceanic fronts have shown that cold/fresh intrusions sink while warm/salty intrusions rise across isopycnals (Horne 1978; Joyce, Zenk & Toole 1978; Gregg & McKenzie 1979), consistent with Stern's (1967) prediction.

These intrusions have also been studied in the laboratory. Thorpe, Hutt & Soulsby (1969) and Chen, Briggs & Wirtz (1971) have made laboratory experiments on stably stratified salt water heated and cooled through side boundaries. They have found alternating layers of cellular motion that extend from one boundary to the other, and Chen *et al.* suggested that the vertical scale of these layers can be scaled by $g\alpha\Delta T/N_s^2$, where g is the acceleration due to gravity, α the thermal-expansion coefficient, ΔT the temperature difference between the heated and the cooled boundaries, and N_s the Brunt–Väisälä frequency for the salt stratification.

Recently, a laboratory experiment that seems to be more relevant to the case of the oceanic front was suggested by Turner (1978) and performed by Ruddick & Turner (1979, herinafter referred to as RT). They prepared two fluids, one on either side of a vertical barrier, which was located halfway across a rectangular tank. One of the fluids was stably stratified with salt and the other with sugar, and both had the same constant density stratification.† At a certain instant the barrier was carefully withdrawn, and a front across which there existed concentration differences of sugar and salt was produced. The concentration differences of sugar and salt increased linearly with local depth z_f (the downward distance from the free surface).‡

Although ideally there should be no density difference across the front, a slight unbalance of the densities at both sides was inevitable. This produced considerable internal gravity waves immediately after the withdrawal of the barrier. These waves, however, decayed away within a few minutes. Then intrusions started to develop from each side with a typical timescale of a few minutes and penetrated into the other fluid. The penetration velocity was nearly proportional to z_f (i.e. the local concentration difference of sugar). The vertical scale of the intrusion was also proportional to z_f. According to RT, these features of the intrusions did not depend on the initial disturbances, which were produced rather randomly by the withdrawal of the barrier.

Based on an assumption that 'sugar fingers' play a dominant role in transporting sugar and salt vertically, RT developed an energy argument to derive the possible vertical scale H of the intrusions and found that H should be between $2(1-\gamma_{su})g\beta_{su}\Delta S_u/N^2$ and $4(1-\gamma_{su})g\beta_{su}\Delta S_u/N^2$, with β_{su} the sugar contraction coefficient, $2\Delta S_u$ the local concentration difference of sugar, N the Brunt–Väisälä frequency for the density stratification, and γ_{su} the ratio of the density flux of salt to that of sugar. Since most of the experimental results for H fell in the above interval, they concluded that the vertical scale of the intrusion can be scaled by $g(1-\gamma_{su})\beta_{su}\Delta S_u/N^2$.

Although the energy argument seems to work well in determining the vertical scale of the intrusions, it assumes the presence of layered intrusions from the beginning and does not require any knowledge of the structure of the intrusions, nor does it

† The diffusivity of salt is about three times as large as that of sugar. Since a salt–sugar system is much easier to handle than a heat–salt system, and yet produces analogous features to those in a heat–salt system, laboratory experiments on double-diffusive phenomena are often performed with a salt–sugar system.

‡ They performed three additional experiments in which the concentration differences of sugar and salt were constant with z_f (see §2.1).

give any information on the structure. Thus it is desirable to develop a theory that explains the vertical scale as well as the behaviour of the intrusions, such as the growth rate, the flow pattern, and salinity and temperature fields. The fact that the development of the intrusions is not influenced by the initial disturbance suggests that those intrusions may be generated as a result of an instability.

Recently, Toole & Georgi (1981, hereinafter referred to as TG) developed a linear stability theory similar to Stern's (1967) theory. They considered a stably stratified fluid with a uniform compensating horizontal temperature and salinity gradients extending to infinity. Although they tried to apply their results to RT's experiment, the wavelength of the fastest-growing mode did not agree with RT's vertical scale, which suggests that the behaviour of a narrow front such as RT's is different from that of TG's front (a front of infinite width). This result is expected, since a front of finite width has a lengthscale based on the concentration differences across the front, but an infinitely wide (as in TG) front does not. It is likely that the behaviour of a front of finite width approaches that of TG's front as the width of the front is increased. However, a criterion that determines whether a front behaves as in RT (a narrow front) or TG (a wide front) has not yet been obtained.

In this paper an attempt is made to interpret the generation of the intrusions found in RT's experiment as a result of an instability of a salinity-temperature front of finite width.† Considering asymptotic limits of infinite and infinitesimal widths, the conditions under which the nature of the front resembles that of RT or that of TG are also derived.

2. Formulation of the problem

2.1. *Basic field*

We consider a salinity–temperature front of finite width that has the following distributions of temperature $\overline{T}$ and salinity $\overline{S}$ (see figure 1):

$$\overline{T} = \frac{N^2}{g\alpha}(\zeta+1)z+\frac{\beta}{\alpha}f(x)\,\Delta S, \tag{2.1}$$

$$\overline{S} = \frac{N^2}{g\beta}\zeta z+f(x)\,\Delta S, \tag{2.2}$$

where

$$f(x) = \begin{cases} 1 & (x > a), \\ x/a & (|x| < a), \\ -1 & (x < -a). \end{cases} \tag{2.3}$$

The x- and z-axes are taken in the cross-frontal and vertical directions respectively. The overbar denotes quantities of the basic field. It can be seen that horizontal gradients of the temperature and salinity are confined to the region given by $|x| < a$, where a is the half-width of the front. The temperature and salinity differences across the front are constant with depth, and are given by $2(\beta/\alpha)\,\Delta S$ and $2\Delta S$ respectively, where β is the salinity contraction coefficient. Since the density $\overline{\rho}$ is given by $\overline{\rho} = \rho_0[1-\alpha(\overline{T}-T_0)+\beta(\overline{S}-S_0)]$, with reference density, temperature and salinity, ρ_0, T_0 and S_0 respectively, there is no horizontal gradient of the density. The temperature

† Although sugar and salt were used in RT's experiment instead of salt and temperature, description will be hereinafter made in terms of salt and temperature to avoid confusion; i.e. 'salt' denotes the slower-diffusing component and 'temperature' the faster-diffusing one.

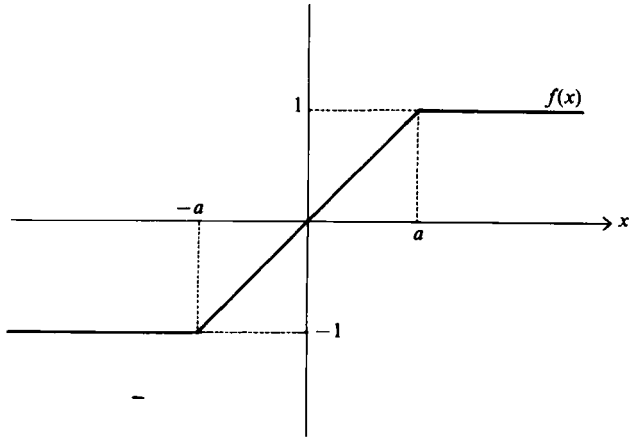

FIGURE 1. Profile of the function $f(x)$ that gives the cross-frontal distributions of the temperature and salinity in the basic field.

and salinity have constant vertical gradients and produce a stable vertical stratification of the density characterized by the Brunt–Väisälä frequency $N = [-(g/\rho_0)\partial\overline{\rho}/\partial z]^{\frac{1}{2}}$. The parameter $\zeta := (g\beta\partial\overline{S}/\partial z)/N^2$ gives the ratio of the density stratification due to salinity to the total density stratification. If $\zeta > 0$ the basic field can support salt fingers. If $-1 < \zeta < 0$ it is absolutely stable, and if $\zeta < -1$ it can support diffusive convections.

We may consider the front given by (2.1)–(2.3) as a crude model of the field in RT's experiment immediately after the internal gravity waves have died down. The mixing that occurred when the barrier was withdrawn has already spread the initial sharp front to one of finite width.

In addition to the experiments described in §1, Ruddick & Turner (1979) performed three extra experiments for the configuration in which ΔS is constant with z_f (see table 1). For these experiments, they found that the vertical scales of the intrusions did not have a systematic dependence on z_f but were again scaled by $g(1-\gamma)\beta\Delta S/N^2$, where γ is the density flux ratio of temperature to salt. Although most of RT's experiments were made for the configuration in which ΔS was proportional to z_f, we shall avoid the complexity that is introduced by considering a linear dependence of ΔS on z_f. Once the behaviours of the intrusions are found for constant ΔS, however, it may be possible to infer those for the case in which ΔS is proportional to z_f by replacing ΔS by its local value.

2.2. *Governing equations*

Consider a disturbance of infinitesimal amplitude superposed on the basic field, and assume that the disturbance has a lengthscale much larger than that of the salt fingers. Then the evolution of the disturbance may be described by the following equations:

$$\frac{\partial u}{\partial t} = -\frac{\partial p}{\partial x} + \epsilon\kappa_e \frac{\partial^2 u}{\partial z^2}, \tag{2.4}$$

$$0 = -\frac{\partial p}{\partial z} + g(\alpha T - \beta S), \tag{2.5}$$

$$\frac{\partial u}{\partial x} + \frac{\partial w}{\partial z} = 0, \tag{2.6}$$

$$\frac{\partial T}{\partial t}+u\frac{\partial \overline{T}}{\partial x}+w\frac{\partial \overline{T}}{\partial z}=\frac{\beta}{\alpha}\gamma\kappa_{\mathrm{e}}\frac{\partial^2 S}{\partial z^2}, \tag{2.7}$$

$$\frac{\partial S}{\partial t}+u\frac{\partial \overline{S}}{\partial x}+w\frac{\partial \overline{S}}{\partial z}=\kappa_{\mathrm{e}}\frac{\partial^2 S}{\partial z^2}, \tag{2.8}$$

where u and w are the velocities in the x- and z-directions respectively, p the kinematic pressure, T the temperature and S the salinity.

The following assumptions and approximations are made to derive the above equations.

(i) Two-dimensionality is assumed, since it can be expected that a disturbance which has a y-dependence has a smaller growth rate.

(ii) The Boussinesq approximation is used.

(iii) The hydrostatic approximation is used, since the aspect ratio of the intrusion found in RT's experiment seems to be fairly small. In fact, it will be shown in Appendix B that non-hydrostatic effects are not significant in RT's experiment except immediately after the barrier has been withdrawn.

(iv) In order to express the effect of enhanced vertical mixing of the temperature and the salinity due to salt fingers, Stern's parametrizations are used: i.e. the salt flux is assumed to be given by $-\kappa_{\mathrm{e}}\,\partial S/\partial z$, where κ_{e} is a constant eddy diffusivity, while the temperature flux is assumed to be proportional to the salt flux with a constant of proportionality $(\beta/\alpha)\gamma$. The value of γ has been measured in so-called run-down experiments by several authors. Recent measurements suggest that γ is not a constant and is a function of the density-anomaly ratio r, which is defined as the ratio of the temperature difference to the salinity difference in the vertical direction (Schmitt 1979; Griffiths & Ruddick 1979; McDougall & Taylor 1984). For $r < 2$, for example, the value of γ seems to be 0.65–0.70 for the temperature–salt problem (Schmitt 1979; McDougall & Taylor 1984) and 0.88–0.92 for the salt–sugar problem (Griffiths & Ruddick 1979). In what follows, however, we shall assume for simplicity that γ is a constant.

(v) In order to retain the possibility that the salt fingers transfer some horizontal momentum, it is also assumed that there is an eddy-momentum flux given by $-\epsilon\kappa_{\mathrm{e}}\,\partial u/\partial z$. However, we have not excluded the possibility that the momentum is transferred principally by a molecular process. For simplicity, $\epsilon = \nu/\kappa_{\mathrm{e}}$ is assumed to be constant, and may be termed a Schmidt number, where ν is either molecular kinematic viscosity ν_{m} or eddy kinematic viscosity ν_{e}.

The parametrizations (iv) and (v) may be applied to the salt-finger interfaces but neglect the presence of the diffusive interfaces. Since the intrusions in RT's experiment have a tilt that indicates that they are driven by the salt-finger process (Turner 1978), however, it is assumed that the absence of the diffusive interfaces is not essential to the dynamics of the intrusions. The effect of the diffusive interfaces will be discussed in §4.

The parametrizations (iv) and (v) also assume the presence of the salt fingers from the beginning. Within the framework of a linear theory, this requires that the basic field is 'finger-sense' stratified. Therefore we shall hereinafter consider the case $\zeta \geqslant 0$ only.

2.3. *Method of solution*

Consider a wave disturbance whose vertical wavenumber is m. Then any variable, say η, can be expressed as

$$\eta = \mathrm{Re}\,[\hat{\eta}(x)\,\mathrm{e}^{\mathrm{i}mz+\sigma t}], \tag{2.10}$$

where Re[ ] denotes real part. σ is the eigenvalue to be determined, and can in general be a complex number. In this paper, however, we shall look for a real positive eigenvalue, which seems relevant to the intrusion problem. Thus σ may be termed the growth rate.

Substituting (2.10) into (2.4) and (2.6)–(2.8), we can express all the variables in terms of p:

$$u = -\mathrm{i}m\psi = -\frac{1}{\sigma+\epsilon\kappa_e m^2}p', \tag{2.11}$$

$$w = \psi' = \frac{1}{\mathrm{i}m(\sigma+\epsilon\kappa_e m^2)}p''. \tag{2.12}$$

$$S = \frac{1}{(\sigma+\kappa_e m^2)(\sigma+\epsilon\kappa_e m^2)}\left[f'p'\Delta S - \frac{N^2\zeta}{\mathrm{i}mg\beta}p''\right] \tag{2.13}$$

$$T = \frac{1}{\sigma}\left\{\frac{\sigma+(1-\gamma)\kappa_e m^2}{\sigma+\kappa_e m^2}\frac{\beta\Delta S}{\alpha}\frac{1}{\sigma+\epsilon\kappa_e m^2}f'p' - \frac{N^2}{\alpha g}\frac{p''}{\mathrm{i}m(\sigma+\epsilon\kappa_e m^2)}\right.$$
$$\left. - \frac{N^2}{\alpha g}\frac{[\sigma+(1-\gamma)\kappa_e m^2]\zeta}{\mathrm{i}m(\sigma+\kappa_e m^2)(\sigma+\epsilon\kappa_e m^2)}p''\right\}, \tag{2.14}$$

where ψ is the stream function and $' := \mathrm{d}/\mathrm{d}x$. The hat $\hat{}$ has been dropped.

Substitution of (2.11)–(2.14) into (2.5) gives a second-order differential equation for p:

$$p'' - \frac{\mathrm{i}\tilde{g}\kappa_e m^3}{[\sigma+(1+\mu)\kappa_e m^2]N^2}f'p' - \frac{m^2\sigma(\sigma+\epsilon\kappa_e m^2)(\sigma+\kappa_e m^2)}{[\sigma+(1+\mu)\kappa_e m^2]N^2}p = 0, \tag{2.15}$$

where $\tilde{g} = \beta\Delta S(1-\gamma)g$ and

$$\mu = (1-\gamma)\zeta. \tag{2.16}$$

Now we non-dimensionalize (2.15) in the following way:

$$x = ax_*, \quad m = d^{-1}m_*, \quad \sigma = \kappa_e d^{-2}\sigma_*, \tag{2.17}$$

where the asterisk denotes dimensionless quantities and

$$d = \tilde{g}/N^2. \tag{2.18}$$

Dropping the asterisks, we obtain

$$p'' - \mathrm{i}Lf'p' - k^2p = 0, \tag{2.19}$$

where

$$L = m^3/[\sigma+(1+\mu)m^2], \tag{2.20}$$

$$k = m\left\{\frac{[\sigma(\sigma+\epsilon m^2)(\sigma+m^2)]}{G[\sigma+(1+\mu)m^2]}\right\}^{\frac{1}{2}} \tag{2.21}$$

and

$$G = N^2d^6/\kappa_e^2a^2. \tag{2.22}$$

It can be seen from (2.19)–(2.22) and (2.3) that the stability of the front is described by three external parameters: G, μ and the Schmidt number ϵ. G will turn out to be most important stability parameter in an inviscid flow ($\epsilon = 0$), and will be termed a frontal stability parameter. μ will be termed a stratification parameter, since it is related to ζ through (2.16). As mentioned in §2.1, we shall only consider the case $\mu \geqslant 0$.

The solutions of (2.19) for $x > 1$ and $x < -1$ are given by

$$p = A\exp(-kx) \quad (x > 1) \tag{2.23}$$

and

$$p = B\exp(kx) \qquad (x > -1), \tag{2.24}$$

where A and B are complex constants. On the other hand, the solution for $|x| < 1$ is given by

$$p = C\exp(in_1 x) + D\exp(in_2 x), \tag{2.25}$$

provided that n_1 and n_2 are not equal,† where $n_1 = \frac{1}{2}[L+(L^2-4k^2)^{\frac{1}{2}}]$ and $n_2 = \frac{1}{2}[L-(L^2-4k^2)^{\frac{1}{2}}]$.

These solutions (2.23)–(2.25) must be matched at $x = \pm 1$. The matching conditions are that the pressure and the horizontal velocity be continuous, i.e.

$$p \text{ is continuous} \tag{2.26}$$

and

$$p' \text{ is continuous.‡} \tag{2.27}$$

Applying these conditions at $x = \pm 1$, we obtain the following equation for the eigenvalue σ:

$$2k^2\{\exp[i(L^2-4k^2)^{\frac{1}{2}}] - \exp[-i(L^2-4k^2)^{\frac{1}{2}}]\}$$
$$+ ik(L^2-4k^2)^{\frac{1}{2}}\{\exp[i(L^2-4k^2)^{\frac{1}{2}}] + \exp[-i(L^2-4k^2)^{\frac{1}{2}}]\} = 0. \tag{2.28}$$

When $L^2-4k^2 < 0$, (2.28) can be written as

$$\tanh(4k^2-L^2)^{\frac{1}{2}} = -(4k^2-L^2)^{\frac{1}{2}}/2k. \tag{2.29}$$

Since k and $(4k^2-L^2)^{\frac{1}{2}}$ are positive, however, (2.29) has no solution. When $L^2-4k^2 > 0$, on the other hand, we have

$$\tan(L^2-4k^2)^{\frac{1}{2}} = -(L^2-4k^2)^{\frac{1}{2}}/2k$$

or

$$\tan\left\{\frac{m^6}{[\sigma+(1+\mu)m^2]^2} - \frac{4m^2\sigma(\sigma+\epsilon m^2)(\sigma+m^2)}{G[\sigma+(1+\mu)m^2]}\right\}^{\frac{1}{2}}$$
$$= -\left\{\frac{Gm^4}{4\sigma(\sigma+\epsilon m^2)(\sigma+m^2)[\sigma+(1+\mu)m^2]} - 1\right\}^{\frac{1}{2}}. \tag{2.30}$$

In § 3 the behaviour of the eigenvalue is examined by solving (2.30).

3. Results

3.1. *Analytical considerations on the behaviour of the eigenvalues*

Before presenting the results of the numerical calculation of the eigenvalues, we shall consider analytically some properties of the eigenvalues based on (2.30).

If we denote by σ_n, the values of σ for which the argument of the tangent in (2.30) become $\frac{1}{2}n\pi$ $(n = 0, 1, \ldots)$ the equation for σ_n is

$$\frac{m^6}{[\sigma_n+(1+\mu)m^2]^2} = \frac{4m^2\sigma_n(\sigma_n+\epsilon m^2)(\sigma_n+m^2)}{G[\sigma_n+(1+\mu)m^2]} + \frac{n^2\pi^2}{4}. \tag{3.1}$$

The behaviour of σ_n can be examined graphically. Figure 2 shows the function $F(\sigma) = m^6/[\sigma+(1+\mu)m^2]^2$ (dashed line) and the functions $G_n(\sigma) = 4m^2\sigma(\sigma+\epsilon m^2)(\sigma+m^2)/G[\sigma+(1+\mu)m^2] + \frac{1}{4}n^2\pi^2$ $(n = 0, 1, \ldots)$ (solid lines) against σ. The curves are drawn schematically for $(1+\mu)\pi < m < \frac{3}{2}(1+\mu)\pi$. Since we are

† When $L^2 = 4k^2$ the solution for $|x| < 1$ must be changed to $p = C\,e^{ikx} + Dx\,e^{ikx}$. Applying the matching conditions (2.26) and (2.27) to this solution and the solutions (2.23)–(2.24), we obtain $2k^2 + k = 0$. Since k is positive, however, this equation has no solution.

‡ This condition can be also obtained by integrating (2.19) between $x = \pm 1-\kappa$ and $\pm 1+\kappa$ $(\kappa \ll 1)$.

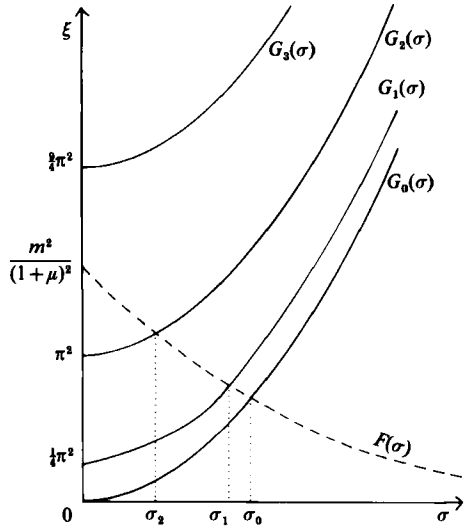

FIGURE 2. Graphs of $F(\sigma)$ and $G_n(\sigma)$ when m is between $(1+\mu)\pi$ and $\frac{3}{2}(1+\mu)\pi$. $F(\sigma)$ is shown by the dashed line and $G_n(\sigma)$ by the solid lines. $F(\sigma)$ intersects the vertical axis (the ξ-axis) at $\xi = m^2/(1+\mu)^2$, while $G_n(\sigma)$ intersects it at $\xi = \frac{1}{4}n^2\pi^2$. The value of σ at the point where $F(\sigma)$ intersects $G_n(\sigma)$ gives σ_n.

considering the case $\mu \geqslant 0$, $F(\sigma)$ is a monotonically decreasing function of σ, and $G_n(\sigma)$ is a monotonically increasing function of σ. The points where $F(\sigma)$ intersects $G_n(\sigma)$ give σ_n, the roots of (3.1). σ_0 exists for all values of m, and the condition for the existence of σ_n is given by $m^2 > \frac{1}{4}(1+\mu)^2 n^2\pi^2$, since $F(0) = m^2/(1+\mu)^2$ and $G_n(0) = \frac{1}{4}n^2\pi^2$.

Now the left- and right-hand sides of (2.30) are shown by the solid lines and the dashed line respectively in figure 3. The curves are drawn schematically for $2(1+\mu)\pi < m < \frac{5}{2}(1+\mu)\pi$. The points where the dashed line intersects the solid lines give the eigenvalues. Note that $\sigma = \sigma_0$ is not an eigenvalue, since $L^2 - 4k^2$ vanishes when $\sigma = \sigma_0$. From figure 3 we can deduce the following important facts.

(i) If σ_{2l+1} $(l = 0, 1, 2, \ldots)$ exists then an eigenvalue σ exists between σ_{2l+2} and σ_{2l+1} (if σ_{2l+2} exists) or between 0 and σ_{2l+1} (if σ_{2l+2} does not exist).

(ii) Since existence of σ_{2l+1} depends only on the value of m, so does the number of the eigenvalues. It is equal to $\langle m/(1+\mu)\pi + \frac{1}{2}\rangle$, where $\langle\ \rangle$ is Gauss's notation for denoting the largest integer that is smaller than $m/(1+\mu)\pi + \frac{1}{2}$.

(iii) There is no eigenvalue for $m > m_c = \frac{1}{2}(1+\mu)\pi$, where m_c will be termed the critical wavenumber. When $m < m_c$, σ_1 does not exist. The left- and right-hand sides of (2.30) respectively increase and decrease monotonically as σ decreases from σ_0. Thus the dashed and solid lines do not intersect except at $\sigma = \sigma_0$. The minimum value of the critical wavenumber is realized for $\mu = 0$ and is equal to $\frac{1}{2}\pi$. This result coincides with the energy argument of RT that the height of the intrusion cannot exceed $4d$.†

(iv) The eigenvalue σ of the fastest-growing mode exists between σ_2 and σ_1 if $m > (1+\mu)\pi$ (or between 0 and σ_1 if $\frac{1}{2}(1+\mu)\pi < m < (1+\mu)\pi$).

(v) The front is always unstable, even if viscosity is present; i.e. there is no marginal stability curve.

† RT's d is equal to $[2(1-\gamma)]^{-1}$ times our d.

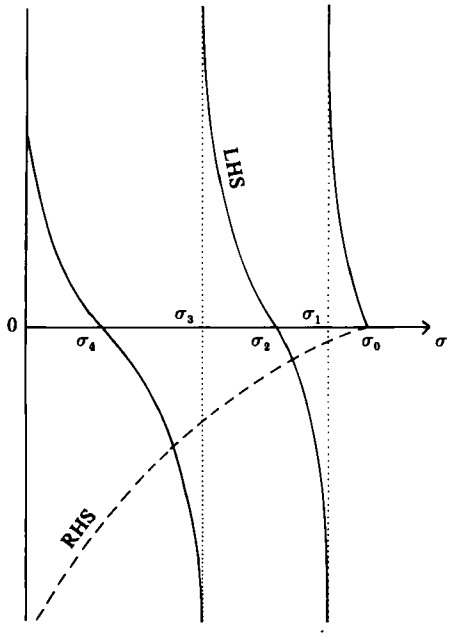

FIGURE 3. Graphs of the right- and left-hand sides of (2.30) for $2(1+\mu)\pi < m < \frac{5}{2}(1+\mu)\pi$. The right-hand side (RHS) is shown by the dashed line and the left-hand side (LHS) by the solid lines. The solid lines intersect the σ-axis at $\sigma = \sigma_{2n}$ $(n = 0, 1, 2, \ldots)$, while they tend to infinity at $\sigma = \sigma_{2n+1}$. The values of σ at the points where the dashed line intersects the solid lines give the eigenvalues.

The above facts make it possible to derive the asymptotic behaviour of the eigenvalue for high wavenumbers. Let us assume that $\sigma_n \sim m^\alpha$ as $m \to \infty$, where α is a constant to be determined. G and ϵ are assumed to be $O(1)$ quantities. If α is larger than 2 it can be shown that (3.1) has no solution. If α is less than 2, on the other hand, (3.1) becomes

$$\frac{m^2}{(1+\mu)^2} = \begin{cases} \dfrac{4m^2\sigma_n^2}{G(1+\mu)} & (\epsilon = 0), \\ \dfrac{4\epsilon m^4 \sigma_n}{G(1+\mu)} & (\epsilon \neq 0), \end{cases} \tag{3.2}$$

which in turn gives

$$\sigma_n \to \begin{cases} \left[\dfrac{G}{4(1+\mu)}\right]^{\frac{1}{2}} - \dfrac{G(2+\mu)}{2(1+\mu)^2} m^{-2} + O(m^{-4}) & (\epsilon = 0) \\ \dfrac{G}{4\epsilon(1+\mu)} m^{-2} + O(m^{-4}) & (\epsilon \neq 0) \end{cases} \tag{3.3}$$

Thus it is expected that when viscosity is absent the growth rate increases and approaches the asymptotic value $[G/4(1+\mu)]^{\frac{1}{2}}$ as the wavenumber becomes large. If viscosity is present, however, the growth rate eventually becomes small for high wavenumbers. It can also be seen that the effect of μ is to reduce the growth rate for high wavenumbers; i.e. the basic salinity stratification in which salinity increases linearly upward has a stabilizing effect.

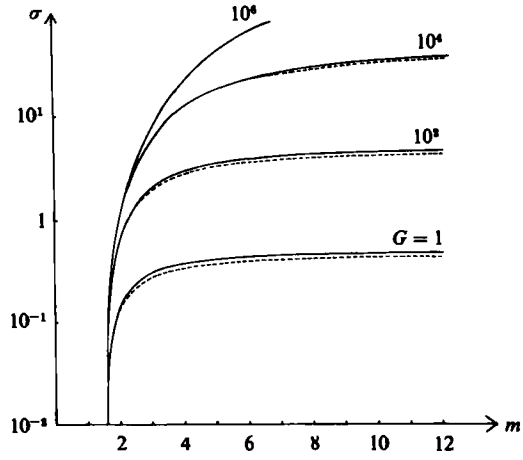

FIGURE 4. The growth rate as a function of the wavenumber for $G = 1$, 10^2, 10^4 and 10^6, when $\epsilon = 0$ and $\mu = 0$. The solid lines show the growth rate under the hydrostatic approximation and the dashed lines the growth rate without the approximation ($\delta = 1.0$).

3.2. *Results of numerical calculations*

The eigenvalue (growth rate) was calculated from (2.30) by using Newton's iterative method for various combinations of G, μ and ϵ. As the initial guess for the eigenvalue, the average of σ_1 and σ_2, which were also calculated from (3.1) by Newton's method, was used.

Figure 4 shows the growth rate (solid lines) as a function of the vertical wavenumber m for various values of G when viscosity is absent and $\mu = 0$. It can be seen that the growth rate increases with increasing G. For a fixed value of G the growth rate increases with the wavenumber and approaches the asymptotic value $\frac{1}{2}G^{\frac{1}{2}}$ predicted by (3.3). The most important feature of this figure, however, is that more than half of the asymptotic value is attained for $m < 10$ when $G < 10^5$. Since motions associated with high wavenumbers are expected to be damped when there is some viscosity, this feature suggests that our choice of the vertical scale in (2.17) was correct, at least for $G < 10^5$. In fact, if the effect of viscosity is included, a maximum in the growth rate is produced at a moderate value of m. Such an example is shown in figure 5 for $\epsilon = 1.0$, $\mu = 0$ and for $G = 1$, 10^2, 10^4 and 10^6. It can be seen that the growth rate again increases with G. The wavenumber of the fastest-growing mode (hereinafter abbreviated as FGM) also increases with G.

The growth rates when the hydrostatic approximation is not used are shown by the dotted lines in figures 4 and 5 (see Appendix B). As shown in Appendix B, the non-hydrostatic effects depend on the parameter $\delta = d/a = g(1-\gamma)\beta\Delta S/N^2a$. The dotted lines in these figures are obtained for $\delta = 1.0$, which seems to be a typical value in RT's experiment.† Figures 4 and 5 suggest that the non-hydrostatic effects are not significant for RT's experiment, and for this reason the results will hereinafter be shown only for the hydrostatic case.

The streamlines, temperature, salinity and buoyancy fields of the FGM for $\epsilon = 2.0$, $\mu = 0$, $G = 10^4$ and $m = 6.4$, and the corresponding total temperature and salinity fields in which the maximum amplitude of the temperature perturbation is assumed

† The initial width of the front in RT's experiment seems to be of order d (see §4.1).

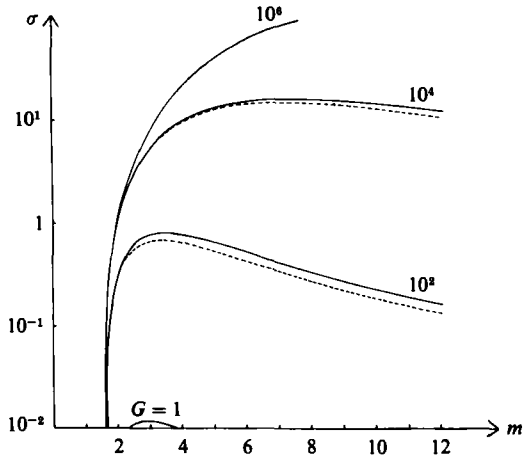

FIGURE 5. Same as figure 4 but $\epsilon = 1.0$.

to be $0.44(\beta\Delta S/\alpha)$, are shown in figures 6(*a–f*) respectively. The direction of the tilt of the intrusion is in the same sense as that of the isotherms of the basic field, as RT observed in their experiment. The cold/fresh water is sinking and the warm/salty water is rising, which is characteristic of the intrusion driven by salt fingers (Turner 1978). Furthermore, the amount of tilt is about one wavelength across the front. This is also similar to what was observed in RT's experiment (see RT's figure 3*a*). However, a qualitative difference is found for the circulation pattern. The theory predicts an alternation of the clockwise and counterclockwise circulations in the vertical direction, while only clockwise circulations were dominant in their experiment. In RT's experiment the clockwise circulation is associated with the salt-finger interface, and the anticyclonic one with the diffusive interface, which is much thinner than the salt-finger interface. Since the present theory neglects the presence of the diffusive interface, it is unable to produce the asymmetry in the circulation pattern.

The wavenumber of the FGM and the corresponding growth rate for $\mu = 0$ are shown respectively for various values of G and ϵ in figures 7 and 8. Generally speaking, the wavenumber of the FGM decreases as G is decreased and/or ϵ is increased. However, there is an asymptotic wavenumber that gives the smallest wavenumber of the FGM for all combinations of G and ϵ. The asymptotic wavenumber is 2.88 and the corresponding growth rate is given by

$$0.047\,19G/4\epsilon \tag{3.4}$$

(see Appendix A). The growth rate of the FGM also decreases as G is decreased and/or ϵ is increased. For small values of G/ϵ the asymptotic formula (3.4) gives an excellent approximation to the eigenvalue.

The asymptotic relations (3.3) and (3.4) suggest that the parameter R defined by

$$R = \frac{G}{\epsilon} = \frac{N^2 d^6}{\nu\kappa_e a^2} \tag{3.5}$$

may play an important role in determining the stability when $\epsilon \neq 0$. In fact, this turns out to be the case. Figures 9 and 10 show the wavenumber of the FGM and the corresponding growth rate for various values of R and ϵ when $\mu = 0$. It can be seen from figure 9 that the wavenumber of the FGM changes within a factor of two

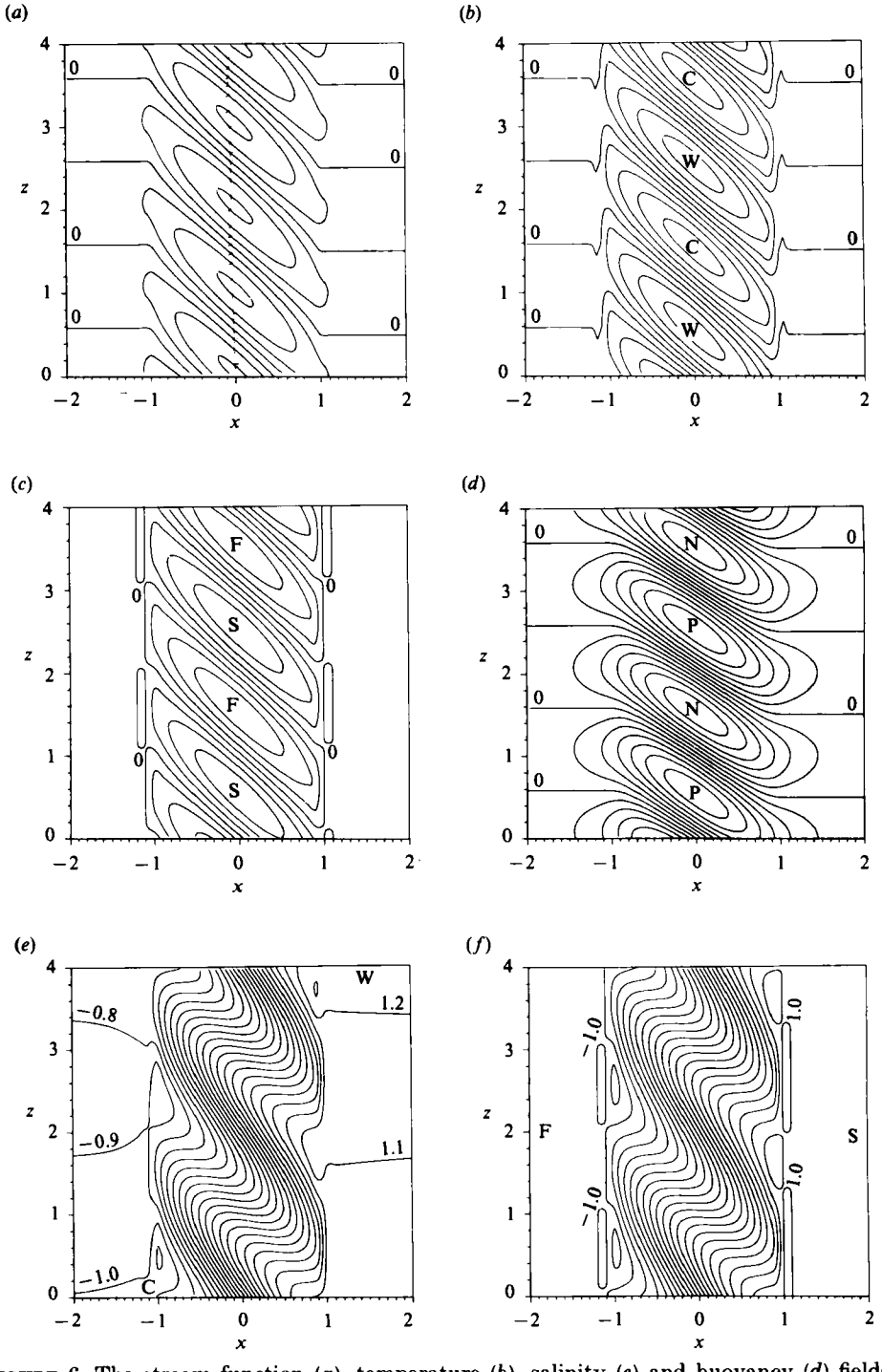

FIGURE 6. The stream function (*a*), temperature (*b*), salinity (*c*) and buoyancy (*d*) fields of the fastest-growing mode for $\epsilon = 2.0$, $\mu = 0$, $G = 10^4$ and $m = 6.4$, and the corresponding total temperature (*e*) and total salinity field (*f*), in which the amplitude of the temperature perturbation is taken to be $0.44\beta\Delta S/\alpha$. The vertical coordinate is scaled by the wavelength $2\pi/m$. Warm salty water is in the right-hand side. C, W, F, S, N and P stand for cold, warm, fresh, salty, negative and positive respectively.

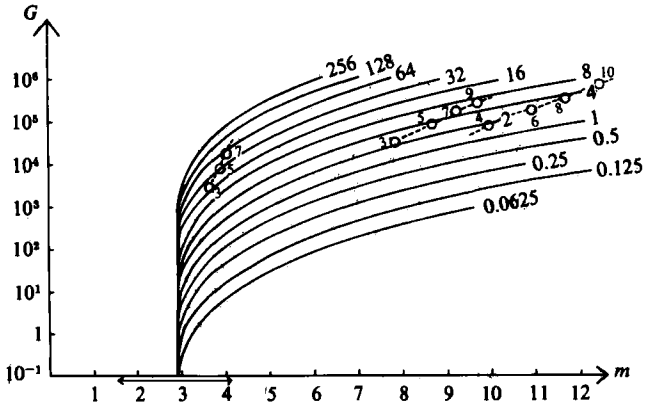

FIGURE 7. The wavenumber of the fastest-growing mode for various values of G and ϵ when $\mu = 0$. The numbers near the curves show the value of ϵ. The wavenumber interval indicated by the arrows near the abscissa shows the range of observed wavenumbers in RT's experiment in which salt concentration increased with the local depth z_t. The dashed lines show the combinations of (G, ϵ) when the scale dependence of the eddy diffusivity is considered. The open circles show the combinations of (G, ϵ) for the integer values of m indicated near the circles.

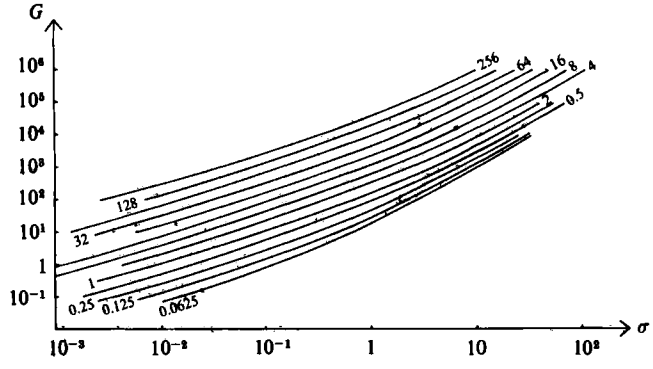

FIGURE 8. The growth rate of the fastest-growing mode for various values of G and ϵ when $\mu = 0$. The numbers near the curves show the value of ϵ.

when ϵ is changed from 10^{-3} to 10^3 for a fixed value of R. Furthermore, the curves for $\epsilon > 10$ almost collapse to the curve for $\epsilon = 10^3$. These features are not seen in figure 7, in which the wavenumber of FGM is plotted against G. Figure 10 also shows that the curves of the growth rate of FGM for $\epsilon > 10$ almost collapse onto the curve for $\epsilon = 10^3$. Such a feature is not seen in figure 8 either. Thus when R is used as a stability parameter instead of G, the dependence of the wavenumber and growth rate of FGM on the Schmidt number is quite weakened.† For this reason, we shall hereinafter show the results in terms of R. The parameter R will be termed a modified frontal stability parameter.

Figure 9 shows that the dependence of the wavenumber of the FGM on R changes according to the value of R. When R is small ($R < 40$) the wavenumber seems to approach a constant asymptotic value for the range of ϵ considered in the present theory (10^{-3}–10^3). The asymptotic value corresponds to a vertical wavelength of $2.2d$.

† This result was suggested by one of the referees.

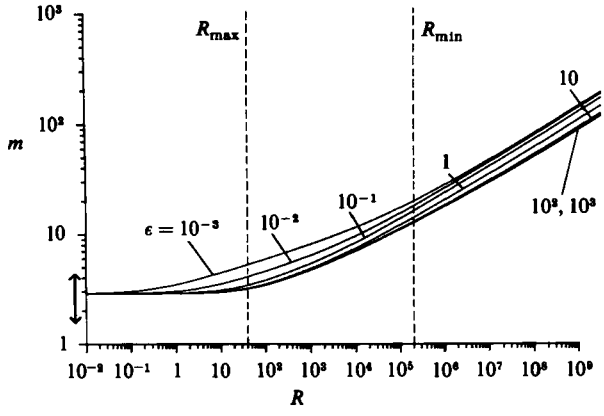

FIGURE 9. The wavenumber of the fastest-growing mode for various values of R and ϵ when $\mu = 0$. The numbers near the curves show the value of ϵ. The wavenumber interval indicated by the arrows near the ordinate shows the range of observed wavenumbers in RT's experiment in which salt concentration increased with z_t. The vertical dashed lines show the values of R_{max} and R_{min}.

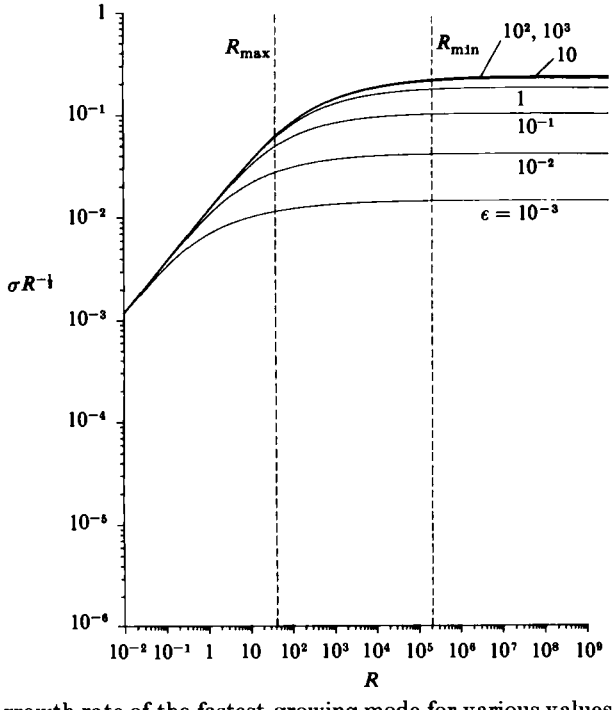

FIGURE 10. The growth rate of the fastest-growing mode for various values of R and ϵ when $\mu = 0$. The ordinate is the growth rate divided by $R^{\frac{1}{2}}$. The numbers near the curves show the value of ϵ. The vertical dashed lines show the values of R_{max} and R_{min}.

Thus Ruddick & Turner's (1979) scaling applies well. When $R > 2 \times 10^5$, on the other hand, the curves tend to be straight lines whose tangent is about $\frac{1}{4}$. This seems to suggest that when R is large the wavenumber tends to be scaled by $d^{-1}R^{\frac{1}{4}}$. Similar features can be seen in figure 10. When R is small the growth rate tends to be proportional to R, in accordance with (3.4). When R is large, on the other hand, it tends to be proportional to $R^{\frac{1}{2}}$.

The wavenumbers and the corresponding growth rates of the FGM for various values of μ are shown in figures 11 (*a–e*) and 12 (*a–e*) respectively. It can be seen from figure 11 that the wavenumber of the FGM increases with increasing μ for small R, but decreases for large R. For a particular value of μ, the dependence of the wavenumber of the FGM on R is similar to that for $\mu = 0$; i.e. the wavenumber becomes independent of R for small R and proportional to $R^{\frac{1}{4}}$ for large R. However, the asymptotic wavenumber for small R increases with increasing μ as predicted by (A 3) in Appendix A. If the regime in which the wavenumber becomes almost constant and the one in which the wavenumber becomes proportional to $R^{\frac{1}{4}}$ are termed the small-R regime and the large-R regime respectively, it can be seen that the transition from the small-R regime to the large-R regime occurs at a larger value of R when μ is larger.

Figure 12 shows that the growth rate of the FGM decreases as μ is increased. The decrease in the growth rate is larger for small R than for large R. The reason why the growth rate decreases as μ is increased can be explained as follows. If (2.7) and (2.8) are combined to give the time rate of change of the buoyancy $g(\alpha T - \beta S)$ we have

$$g\frac{\partial}{\partial t}(\alpha T - \beta S) = -N^2 w - \beta(1-\gamma)\kappa_e \frac{\partial^2 S}{\partial z^2}. \tag{3.6}$$

The first term on the right-hand side arises because the buoyancy is reduced when a fluid particle moves upward against the stable density stratification. The second term on the right-hand side expresses the production of buoyancy through selective transport of temperature and salinity due to salt fingers. Since we are assuming a wavy structure in the vertical direction, this term is proportional to S. On the other hand, the time rate of change of S is governed by (2.8), which shows that the production of S is reduced when there is a positive vertical gradient of $\overline{S}$. Thus, when $\overline{S}_z$ is increased for a fixed value of N^2 (i.e. μ is increased), the production of the buoyancy due to salt fingers is reduced, and so is the growth rate. The case in which the movement of the fluid particle is downward can be discussed similarly, and results in the same conclusion.

Figure 12 also shows that the growth rate is proportional to R for small R (in accordance with the asymptotic analysis in Appendix A) and proportional to $R^{\frac{1}{2}}$ for large R. This feature is similar to that for $\mu = 0$. It is obvious that the regime in which the growth rate is proportional to R and the one in which it is proportional to $R^{\frac{1}{2}}$ correspond respectively to the small-R regime and the large-R regimes.

We shall now try to determine the values of R above and below which the large-R and small-R regimes respectively prevail. If these values of R are denoted respectively by $R_{\min}$ and $R_{\max}$, then the large-R regime prevails for $R > R_{\min}$ and the small-R regime for $R < R_{\max}$. Here we shall define $R_{\max}$ as the value of R above which the wavenumber of the FGM for $\epsilon = 10^{-3}$–10^{3} is more than twice the asymptotic wavenumber for small R. This definition of $R_{\max}$ together with figures 9 and 11 give the following experimental relation between $R_{\max}$ and μ:

$$R_{\max} = 40(1+\mu)^{5.4}. \tag{3.7}$$

On the other hand, $R_{\min}$ may be defined as the value of R above which the wavenumber of the FGM divided by $R^{\frac{1}{4}}$ becomes less than 120 % of its asymptotic value for large R (see the asymptotic analysis in §4.2). This definition of $R_{\min}$ gives

$$R_{\min} = 2\times 10^5(1+\mu)^{4.9}. \tag{3.8}$$

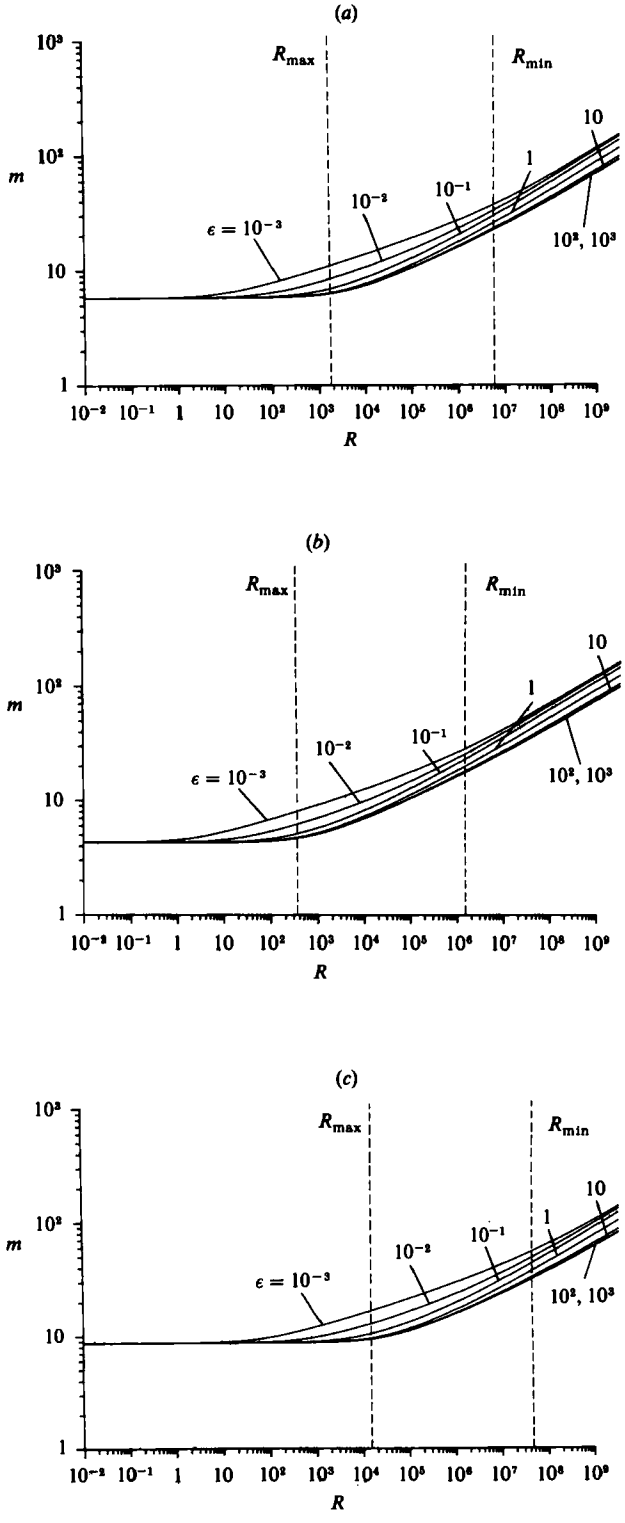

FIGURE 11 (*a–c*). For caption see facing page.

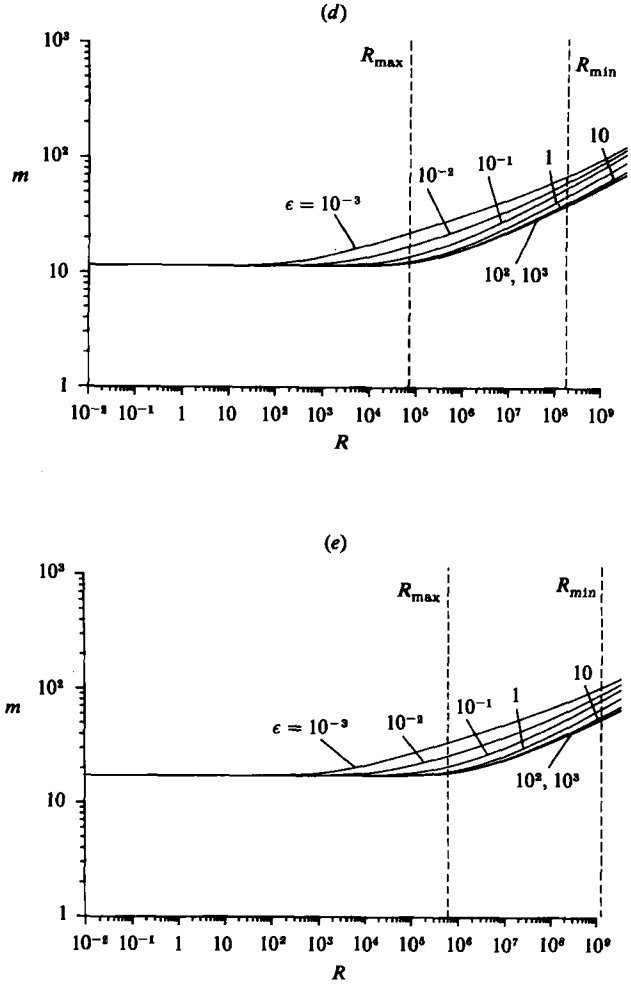

FIGURE 11. The wavenumber of the fastest-growing mode for various values of μ and ϵ: (*a*) $\mu = 0.5$; (*b*) 1.0; (*c*) 2.0; (*d*) 3.0; (*e*) 5.0. The numbers near the curves show the value of ϵ. The vertical dashed lines show the values of R_{max} and R_{min}.

The values of R_{min} and R_{max} are shown by the vertical dashed lines in figures 9–12. It can be seen from figures 10 and 12 that the values of R_{min} and R_{max} determined from the above criteria reasonably separate the small-R regime, in which the growth rate is proportional to R, and the large-R regime, in which it is proportional to $R^{\frac{1}{2}}$, from the transition regime between them.

4. Discussion of the results

4.1. *Comparison with Ruddick & Turner's (1979) experiment*

Table 1 presents the parameters used in RT's three experiments in which the salt-concentration anomaly (ΔS across the front) was constant with depth. As can be seen from the value of ζ in table 1,† the stratification is in the 'diffusive sense'

† These values of ζ were kindly provied by B. R. Ruddick (1984, private communication).

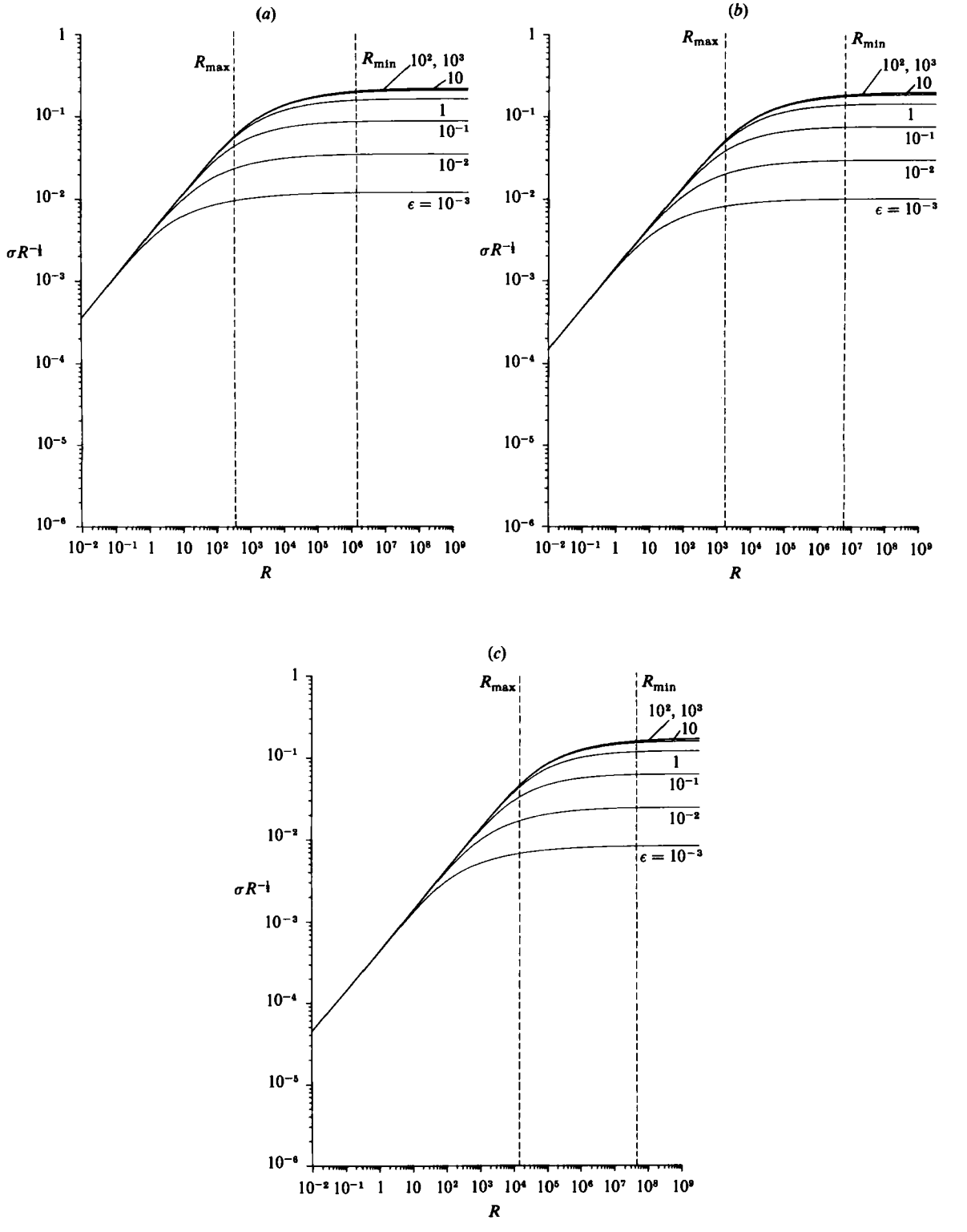

FIGURE 12(*a–c*). For caption see facing page.

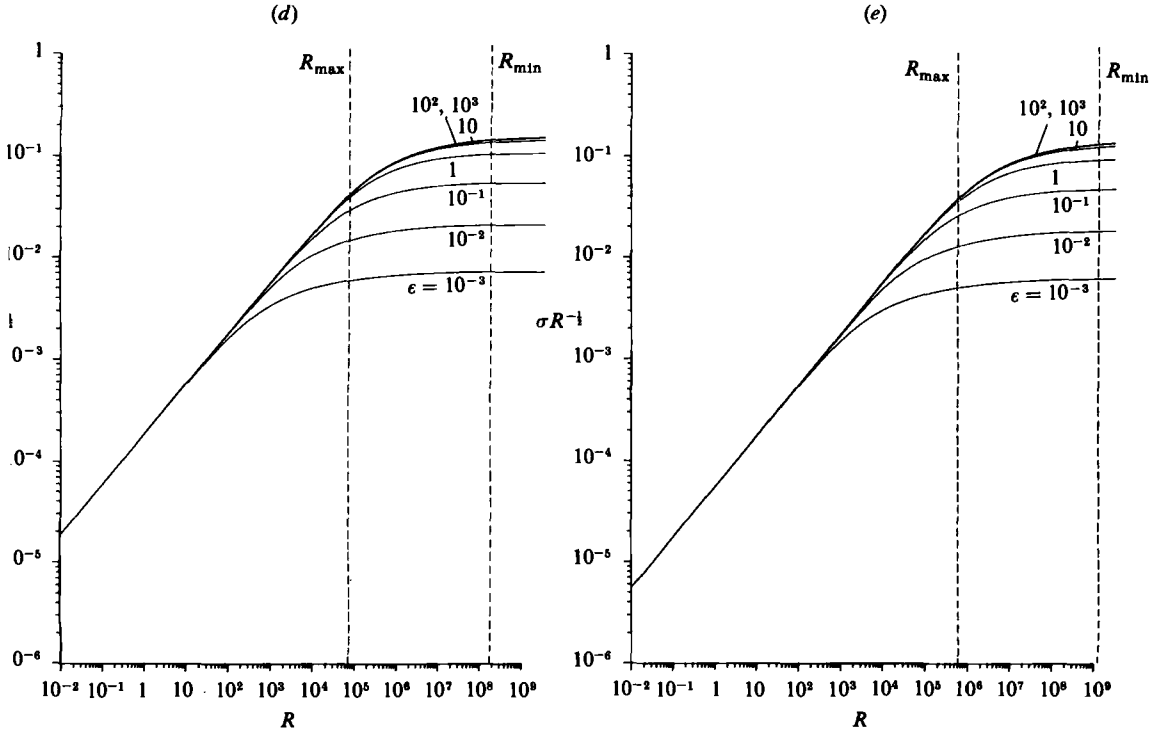

FIGURE 12. The growth rate of the fastest-growing mode for various values of μ and ϵ: (*a*) $\mu = 0.5$; (*b*) 1.0; (*c*) 2.0; (*d*) 3.0; (*e*) 5.0. The ordinate is the growth rate divided by R^4. The numbers near the curves show the value of ϵ. The vertical dashed lines show the values of R_{max} and R_{min}.

	Experiment 1	Experiment 2	Experiment 3
$\beta\Delta S$	0.012	0.0015	0.0055
ζ	0	< -1	1.96
$-1/\rho_0\,\partial\bar{\rho}/\partial z$	1.3×10^{-3}	1.2×10^{-3}	0.67×10^{-3}
d	1.2 cm	0.15 cm	1.0 cm
H	3.0 cm	0.30 cm	2.3 cm
l	2.5	2.0	2.3
m	2.5	3.1	2.7
κ_e	9×10^{-3} cm^2 s^{-1}	4×10^{-4} cm^2 s^{-1}	5×10^{-3} cm^2 s^{-1}
G	3×10^4	4×10^3	3×10^4
d^2/κ_e	2×10^2 s	5×10^1 s	2×10^2 s
ϵ	1	3×10^1	2
R	3×10^4	1×10^2	2×10^4

TABLE 1. Parameters in Ruddick & Turner's (1979) three experiments in which ΔS is constant with z_f

in Experiment 2, and in the 'salt-finger sense' in Experiment 3. There is no salinity stratification in Experiment 1. Strictly speaking, the present linear theory is valid only for the case $\zeta \geqslant 0$, which ensures the presence of salt fingers. Since salt fingers were observed between the intrusions even in Experiment 2, however, a comparison will be also made for this case. $(-1/\rho_0)\,\partial\bar{\rho}/\partial z$ is a measure of the basic density stratification and d is the vertical scale defined by (2.18), where γ is taken to be 0.88

as in RT. H is the height of the intrusion found in the experiments, $l := H/d$ the dimensionless height and m the corresponding dimensionless wavenumber. Since the stratification parameter μ defined by (2.16) is small compared with 1 in RT's experiment because of the factor $1-\gamma$, we shall use only the theoretical results for $\mu = 0$ for the purpose of the comparison to the experimental results.†

In order to compare the theoretical and experimental results, it is necessary to estimate the magnitudes of R and ϵ in the experiment. The modified frontal stability parameter R is defined by

$$R = N^2 d^6/\epsilon\kappa_e^2 a^2, \tag{4.1}$$

where we have three unknown quantities κ_e, a and ϵ. The value of a seems to be determined by the mixing due to initial disturbances. Figure 2 (b) of RT suggests that the horizontal scale of the mixing region is about the same as the height of the intrusions; i.e. $2a \sim H \equiv ld \sim 2d$ (see table 1). Thus we may assume that $a \sim d$.

To estimate the eddy diffusivity of salt due to salt-fingers is a more difficult task. However, we start from the definition of the eddy diffusivity:

$$\kappa_e = \beta F_S/\beta S_z, \tag{4.2}$$

where F_S is the salt flux due to salt fingers and S_z is the vertical gradient of salt concentration across the salt-finger interfaces.

In RT's experiment the vertical stratification of the basic salinity field is not so strong, and the typical salinity change over the height of the intrusions is at least four times smaller than the salinity difference across the front (e.g. in Experiment 3, $\beta(\partial\bar{S}/\partial z)H = 2.7\times10^{-3}$, while $2\beta\Delta S = 0.011$). Therefore the salinity difference across the salt-finger interfaces is likely to be determined by horizontal advection of salinity due to the intrusions and is considered to be of the order of $2\beta\Delta S$.

If we use Stern & Turner's (1969) experimental result to estimate βF_S together with the above estimate of the salinity difference across the salt-finger interfaces, βF_S and βS_z may be given by

$$\beta F_S \approx A(2\beta\Delta S)^{\frac{4}{3}} \tag{4.3}$$

and

$$\beta S_z \approx 2\beta\Delta S/H, \tag{4.4}$$

where A was estimated by Stern & Turner (1969) to be around 10^{-2} g cm^{-2} s^{-1} for salt/sugar fingers. Accurate measurements by Griffiths & Ruddick (1979) also suggest that A is around 10^{-2} for small values of the density-anomaly ratio. Substituting (4.3) and (4.4) into (4.2), we obtain

$$\kappa_e \approx H(2\beta\Delta S)^{\frac{1}{3}}\times10^{-2}\ \text{cm}^2\ \text{s}^{-1}. \tag{4.5}$$

The values of κ_e calculated from (4.5) are shown in table 1 together with the frontal stability parameter G and the diffusion timescale d^2/κ_e, which is used to scale the time in the present theory. The values of κ_e could be smaller than those presented in table 1, since the vertical salinity difference should be less than $2\beta\Delta S$ and also the coefficient A in (4.3) should be smaller than 10^{-2} g cm^{-2} s^{-1}. These estimates of the eddy diffusivity suggest that the eddy diffusivity κ_e is smaller than the molecular kinematic viscosity ν_m.

The vertical momentum-transfer process due to salt fingers is not yet well understood. Let us consider here the ratio of the vertical momentum flux by salt fingers to that by molecular processes: $\overline{u'w'}/\nu_m(\partial u/\partial z)$. If the correlation coefficient

† The effect of salinity stratification can considerably affect the stability of oceanic fronts, where $1-\gamma$ is 0.30–0.35 (Schmitt 1979; McDougall & Taylor 1984).

	Experiment 1	Experiment 2	Experiment 3
m (observed)	2.5	3.1	2.7
m (theory)	9.0	3.4	7.9
e-folding time	6 s	6×10^1 s	1×10^1 s

TABLE 2. Comparison of the wavenumber of the intrusion between the theoretical prediction and the observed value

between u' and w' is denoted by C_1 ($|C_1| < 1$) then the ratio may be written as $C_1 w' H/\nu_m$. If we multiply this expression by $2\Delta S$ then we have

$$C_1 \frac{w' 2\Delta S}{\nu_m (2\Delta S/H)} = \frac{C_1}{C_2} \frac{\overline{w'S'}}{\nu_m (\partial S/\partial z)} = \frac{C_1}{C_2} \frac{\kappa_e}{\nu_m}, \tag{4.6}$$

where C_2 is the correlation coefficient between w' and S'. Since salt fingers are driven by a buoyancy excess due to salt, it is probable that the correlation coefficient C_2 for w' and S' is larger than C_1 for u' and w'. Thus (4.6) suggests that the momentum flux due to salt fingers could be smaller than that due to molecular processes. If the molecular kinematic viscosity ($\nu_m = 10^{-2}$ cm^2 s^{-1}) is used for the viscosity term, then the values of κ_e in table 1 suggest that the Schmidt number ϵ may be between $1\text{–}3 \times 10^1$. Finally, the above estimates of a, κ_e and ϵ gives the value of R listed in table 1.

We shall now compare the theoretical results with experimental values. Given the estimated values of R and ϵ, we can obtain the wavenumber of the FGM from figure 9. This is compared with the observed one in table 2. The predicted scales are found to be about three times smaller than those observed in the experiment except for Experiment 2, where good agreement is seen.

The wavenumber interval indicated by the arrows on the left-hand side of the vertical axis in figure 9 shows the observed wavenumbers in most of RT's experiments in which the salt-concentration anomaly $2\beta\Delta S$ increased with z_f ($2\beta\Delta S = z_f(-1/\rho_0)\partial\overline{\rho}/\partial z$). For these experiments the value of μ is between -0.12 and 0, so that the present linear theory cannot be applied in a strict sense. Since rigorous salt fingers were observed in these experiments, however, we shall try to compare the theoretical and experimental results.† If we estimate a and κ_e in the same manner as described above and take $H \sim 3d$ (see RT's figure 5) then R and ϵ are given by

$$R = \frac{10^4}{54} g(1-\gamma)^3 \left[\frac{-1}{\rho_0}\frac{\partial\overline{\rho}}{\partial z}\right]^{\frac{2}{3}} z_f^{\frac{8}{3}} \tag{4.8}$$

and

$$\epsilon = \tfrac{2}{3}(1-\gamma)^{-1}\left[\frac{-1}{\rho_0}\frac{\partial\overline{\rho}}{\partial z}\right]^{-\frac{1}{3}} z_f^{-\frac{4}{3}}. \tag{4.9}$$

Thus when z_f and/or $(-1/\rho_0)\partial\overline{\rho}/\partial z$ increase, R increases and ϵ decreases. Since the value of z_f and $(-1/\rho_0)\partial\overline{\rho}/\partial z$ in the experiments are respectively between 3 and 25 cm and between 0.33×10^{-3} and 7.5×10^{-3} cm^{-1} (see RT's figure 5), R is between 2.2×10^2 and 1.4×10^5 and ϵ between 0.4 and 6.8. For these values of R and ϵ, figure 9 suggests that the wavenumber of the FGM ranges between 3.6 and 13. Considering

† The present theoretical treatment may be formally valid even for $-1 < \mu < 0$ as far as the presence of salt fingers is ensured, although we shall use the theoretical results for $\mu = 0$ in order to compare with the experimental ones.

	Experiment 1	Experiment 2	Experiment 3
κ_e	$2.19 \times 10^{-2}/m$ cm^2 s^{-1}	$1.34 \times 10^{-2}/m$ cm^2 s^{-1}	$1.38 \times 10^{-2}/m$ cm^2 s^{-1}
G	$5.50 \times 10^3 m^2$	$3.32 \times 10^2 m^2$	$3.44 \times 10^3 m^2$
ϵ	$0.46m$	$7.46m$	$0.72m$
R	$1.2 \times 10^4 m$	$4.4 \times 10^1 m$	$4.7 \times 10^3 m$
m	15.0	3.7	9.7

TABLE 3. The wavenumber of the fastest-growing mode when the scale dependence of the eddy diffusivity is considered

the rough assumptions made in the theory, the agreement seems to be satisfactory. It is especially noteworthy that the theory predicts the right scaling d for the height of the intrusions.

Two possible reasons for the discrepancy between the observed wavenumber and the predicted wavenumber of the FGM may be considered. First, since the intrusion in the experiment is a nonlinear phenomenon, the wavelength could be different by a factor of two or three from what is expected from the linear stability theory. In fact, recent investigations on various instabilities show that the wavenumbers of the observed finite-amplitude waves are different from those of the FGM by a factor of two or three (see e.g. Yoshizaki 1982; Niino & Misawa 1984).

Secondly, the assumption of constant eddy diffusivity may not be appropriate. Based on the assumption that the heat and salt fluxes through salt-finger interfaces dominate those through diffusive ones, Stern's parametrizations in (2.7) and (2.8) neglect the presence of the diffusive interfaces and introduce constant diffusivities of heat and salt everywhere. Although the assumption that the fluxes through the salt-finger interfaces are important is supported by the sense of the tilt of the intrusions in the RT's experiment and leads us to the right scaling for the wavenumber of FGM, the effect of the diffusive interfaces where the effective diffusivity becomes very small but the vertical gradients of velocity, salinity and temperature become large could play a role in determining the precise value of the wavenumber. The effect of the diffusive interfaces remains an important problem to be studied in the near future.

As (4.5) suggests, the eddy diffusivity could also depend on the vertical scale of the intrusions. Although the effects of the scale dependence of the eddy diffusivity cannot be explicitly taken into account in the linear stability theory, they may be examined using (4.5) and figure 7.† For intrusions whose vertical wavenumber is m the eddy diffusivity due to salt fingers is given by

$$\kappa_e = 10^{-2} \frac{2\pi d}{m} (2\beta \Delta S)^{\frac{1}{3}}. \tag{4.7}$$

This produces a wavenumber dependence of ϵ and G as shown in table 3. Figure 7 shows the combinations of (G, ϵ) as functions of m (the dashed lines) for RT's three experiments. The open circles on the dashed lines show the combinations of (G, ϵ) for several integer values of m. The points where the wavenumber on the dashed lines coincides with that of the abscissa is considered to give the wavenumber of the FGM when the scale dependence of the eddy diffusivity is present. The wavenumbers thus

† We shall use figure 7 instead of figure 9 to examine the effect of the scale dependence of the eddy diffusivity on the stability, because figure 7 gives a better resolution for $m < 12$ than does figure 9.

obtained are shown in table 3 for the three experiments. It can be seen that the scale dependence of the eddy diffusivity tends to increase the wavenumber of the FGM. Thus the scale dependence of the eddy diffusivity does not seem to explain the discrepancy.

The theoretical predictions of the growth rates corresponding to the three RT experiments can be obtained from figure 10 and are shown in table 2. The e-folding time for Experiments 1 and 3 is about 10 s, which seems to be somewhat shorter than what was observed in RT's experiments. The e-folding time for Experiment 2 is about 60 s and seems to be in good agrement with experiment. Again, in spite of the crude model assumed in the theory, the agreement seems to be satisfactory.

4.2. *Asymptotic behaviour of the present model: comparison with Toole & Georgi's (1978) model and Ruddick & Turner's (1979) model*

The present results show that, for fixed values of ϵ and μ, the preferred scale of the intrusion becomes independent of R and the growth rate becomes proportional to R when R is small (the small-R regime). When R is large (the large-R regime), on the other hand, the preferred scale becomes proportional to $R^{-\frac{1}{4}}$ and the growth rate to $R^{\frac{1}{2}}$. In order to understand the physical implication of this behaviour, we shall decompose the modified frontal stability parameter R into two dimensionless parameters:

$$R = \lambda^4 \delta^6, \tag{4.9}$$

where

$$\lambda = \frac{a}{(\kappa_e/N)^{\frac{1}{2}} \epsilon^{\frac{1}{4}}} \tag{4.10}$$

and

$$\delta = \frac{d}{a} = \frac{g(1-\gamma)}{N^2} \frac{\mathrm{d}(\beta \overline{S})}{\mathrm{d}x} \tag{4.11}$$

are respectively the dimensionless width of the front and the dimensionless horizontal gradient of salinity in the basic field.

First let us consider the case in which $\lambda \ll 1$ and $\delta = O(1)$ or $\delta \ll 1$ and $\lambda = O(1)$, so that $R \ll 1$; for example the horizontal gradient of the mean salinity may be kept constant and the width of the front decreased, or the width of the front may be kept constant and the horizontal gradient of the mean salinity decreased. When $R \ll 1$ an asymptotic analysis based on (3.1) proceeds exactly in the same manner as described in Appendix A, and the wavenumber and the growth rate of the FGM are given by $2.88(1+\mu)$ and $0.4719R/4(1+\mu)^3$ respectively. Thus the asymptotic analysis explains the behaviour of the wavenumber and the growth rate for small R in figures 9–12. In dimensional units the wavelength corresponding to the asymptotic wavenumber is $2.2d/(1+\mu)$, which is Ruddick & Turner's scale for moderate values of μ. Thus we may call the small-R regime the Ruddick & Turner regime.

The balance of the terms in the basic equations for $R \ll 1$ is given by

$$0 = -\frac{\partial p}{\partial x} + \epsilon \kappa_e \frac{\partial^2 u}{\partial z^2}, \tag{4.12}$$

$$u \frac{\partial \overline{S}}{\partial x} + w \frac{\partial \overline{S}}{\partial z} = \kappa_e \frac{\partial^2 S}{\partial z^2}, \tag{4.13}$$

(2.5), (2.6) and (3.6). The terms involving the time rate of change are not important in comparison with the vertical diffusion terms except in the buoyancy equation. Horizontal and vertical advections of salinity of the basic field due to intrusions are exactly balanced by the vertical transport of salinity due to salt fingers. The

	n
$\beta = 0$	$2m^3/n\pi - m^2(1+\mu)$ $(= O(1))$
$0 < \beta < \frac{1}{8}$	$2m^3/n\pi$ $(= O(R^{3\beta}))$
$\beta = \frac{1}{8}$	$R/32m^2\,[-n^2\pi^2\epsilon + (n^4\pi^4\epsilon^2 + 256R^{-1}m^8\epsilon)^{\frac{1}{2}}]$ $(= O(R^{\frac{3}{8}}))$
$\frac{1}{8} < \beta < \frac{1}{4}$	$m(\epsilon R)^{\frac{1}{4}}/2^{\frac{1}{2}}$ $(= O(R^{\beta+\frac{1}{4}}))$
$\beta = \frac{1}{4}$	$\sigma_0 R^{\frac{1}{2}}$, where σ_0 is given by $m_0^4/\sigma_0 + (1+\mu)m_0^2 = 4\sigma_0(\sigma_0/\epsilon + m_0^2)(\sigma_0 + m_0^2)$
$\beta > \frac{1}{4}$	$R/4(1+\mu)m^2$ $(= O(R^{1-2\beta}))$

TABLE 4. Asymptotic dispersion relations when R tends to infinity

buoyancy is produced through selective transports of heat and salinity due to salt fingers, while it is reduced by ascending or descending against the stable stratification.

Let us now consider the case in which $R \gg 1$. R can be large for $\lambda \gg 1$ and $\delta = O(1)$, or $\lambda = O(1)$ and $\delta \gg 1$. When $\delta \gg 1$, however, several effects that are not considered in the present theory are likely to become important. In particular, non-hydrostatic effects and lateral diffusion effects will have to be considered. The non-hydrostatic effects may be studied by an asymptotic analysis of (B 1) in Appendix B. However, it is not easy to examine the effect of lateral diffusion in the context of the present theory. Therefore we shall hereinafter consider only the case in which $\lambda \gg 1$ and $\delta = O(1)$; i.e. the horizontal gradient of the mean salinity is kept constant and the width of the front is increased to infinity.

Assuming that $\sigma_n = \sigma_0 R^\alpha$ and $m = m_0 R^\beta$ in (3.1), where m_0 and σ_0 are $O(1)$ quantities, we can obtain a hierarchy of asymptotic dispersion relations according to the value of β. These relations are summarized in table 4. It is found from table 4 that the FGM is realized for a wavenumber $O(R^{\frac{1}{4}})$ and has a growth rate $O(R^{\frac{1}{2}})$. The dispersion relation is given by

$$\frac{m_0^4}{\sigma + (1+\mu)m_0^2} = 4\sigma\left(\frac{\sigma}{\epsilon} + m_0^2\right)(\sigma + m_0^2). \tag{4.14}$$

The value of m_0 that maximizes σ_0 for a given value of ϵ and the corresponding value of σ_0 are shown in figure 13 for $\mu = 0$. An asymptotic analysis of (4.14) gives $m_0 \to \{2(1+\mu)^{\frac{1}{2}}[1+(1+\mu)^{\frac{1}{2}}]\}^{-\frac{1}{2}}$ as $\epsilon \to \infty$ and $m_0 \to [(2+\mu)/4(1+\mu)^2]^{\frac{1}{4}}$ as $\epsilon \to 0$. Thus m_0 has a very weak dependence on ϵ. On the other hand, $\sigma_0 \to \frac{1}{2}[1+(1+\mu)^{\frac{1}{2}}]^{-1}$ as $\epsilon \to \infty$ and $\sigma_0 \to \epsilon^{\frac{1}{2}}/2(1+\mu)^{\frac{1}{2}}$ as $\epsilon \to 0$. Figures 9–12 show that the asymptotic relationship (4.14) fits well for $R > 2 \times 10^5(1+\mu)^{4.9}$.

In dimensional units the wavenumber of the FGM is of order $(N^2\delta^2/\epsilon\kappa_e)^{\frac{1}{4}}$ and the growth rate $N\delta\epsilon^{-\frac{1}{2}}$. Therefore the appropriate scaling for $R \gg 1$ is not given by (2.17), but by $\sigma = N\sigma_*$ and $m = (N/\kappa_e)^{\frac{1}{2}}m_*$, which is Toole & Georgi's scaling for a front of infinite width.

If Toole & Georgi's scaling is used for (2.15) with $x = (\kappa_e/N)^{\frac{1}{2}}x_*$ from the beginning, (2.15) becomes

$$p'' - \frac{im^3\delta}{\sigma + (1+\mu)m^2}f'p' - \frac{m^2\sigma(\sigma+\epsilon m^2)(\sigma+m^2)}{\sigma + (1+\mu)m^2}p = 0, \tag{4.15}$$

where

$$f' = \begin{cases} 0 & (x > \lambda), \\ 1 & (|x| < \lambda), \\ 0 & (x < -\lambda). \end{cases}$$

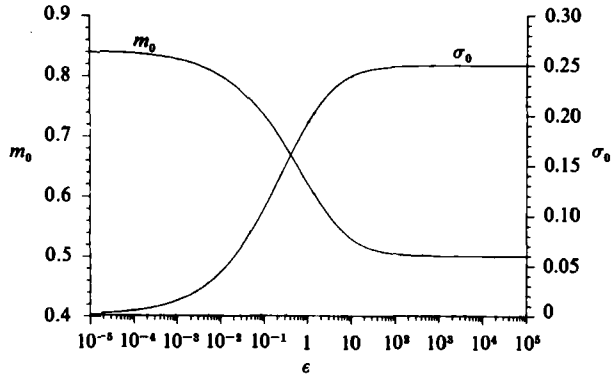

FIGURE 13. m_0 and σ_0 as functions of ϵ for $\mu = 0$.

Then the relationship corresponding to (3.1) becomes

$$\frac{\delta^2 m^6}{[\sigma_n + (1+\mu)\, m^2]^2} = \frac{4m^2\sigma_n(\sigma_n + \epsilon m^2)(\sigma_n + m^2)}{\sigma_n + (1+\mu)\, m^2} + \frac{n^2\pi^2}{4\lambda^2}, \tag{4.16}$$

which gives the following asymptotic relations between the eigenvalue and the wavenumber as $\lambda \to \infty$:

When $m = O(1)$, σ is given by

$$\frac{\delta^2 m^6}{\sigma + (1+\mu)\, m^2} = 4m^2\sigma(\sigma + m^2)(\sigma + \epsilon m^2), \tag{4.17}$$

When $m = O(\lambda^\beta)$ $(\beta > 0)$, on the other hand,

$$\sigma \sim \begin{cases} \dfrac{\delta}{4(1+\mu)} & (\epsilon = 0), \\ \dfrac{\delta^2}{4\epsilon(1+\mu)\, m^2} & (\epsilon \neq 0). \end{cases}$$

Therefore when $\epsilon \neq 0$ the wavenumber of the most unstable mode is $O(1)$ and the dispersion relation is given by (4.17).

The dispersion relation for Toole & Georgi's model in which an infinite front is assumed can be obtained from (4.15) by putting $f' = 1$ for all x and assuming that $p \sim \mathrm{e}^{\mathrm{i}kx}$, where k is the wavenumber in the x-direction:

$$-k^2 + \frac{\delta k m^3}{\sigma + (1+\mu)\, m^2} - \frac{m^2\sigma(\sigma + m^2)(\sigma + \epsilon m^2)}{\sigma + (1+\mu)\, m^2} = 0. \tag{4.18}$$

This equation is the same equation as TG's (20), except that the notation is different.† For a given m, the value of k that maximizes the growth rate may be obtained by differentiating (4.18) with respect to k and assuming $\partial\sigma/\partial k = 0$. This gives

$$k = \frac{m^3\delta}{2[\sigma + (1+\mu)\, m^2]}. \tag{4.19}$$

† The last term ϵ_x in TG's (20) should be ϵ_z. Furthermore, their (20) seems to be derived under the hydrostatic approximation, although they claim that it is derived when *all* the acceleration terms are retained.

Substituting (4.19) into (4.18), we obtain the same dispersion relation as (4.17). Thus Toole & Georgi's model can be recovered as an asymptotic limit ($\lambda \to \infty$) of our model.

It is only left to show that (4.17) coincides with (4.14). If (4.17) is dimensionalized, we have

$$\frac{N^2\kappa_e^2\delta^2 m^6}{\sigma+(1+\mu)\kappa_e m^2} = 4m^2\sigma(\sigma+\epsilon\kappa_e m^2)(\sigma+\kappa_e m^2), \tag{4.20}$$

Again non-dimensionalizing (4.20) according to (2.17),

$$\frac{m^6}{\sigma+(1+\mu)m^2} = \frac{4m^2\sigma(\sigma/\epsilon+m^2)(\sigma+m^2)}{R}. \tag{4.21}$$

This is the same equation as (4.14) if we notice that $m = m_0 R^{\frac{1}{4}}$ and $\sigma = \sigma_0 R^{\frac{1}{2}}$. Therefore, even if the scaling given by (2.17) is used, Toole & Georgi's result can be obtained as an asymptotic limit of $R \gg 1$ in our problem.

This is also observed in the behaviour of the solution. When the dispersion relation (4.18) holds, $L \sim 2k = O(R^{\frac{1}{4}})$ and $(L^2-4k^2)^{\frac{1}{2}} = O(1)$. Therefore the solution in the frontal region is approximately given by $p \sim C\,\mathrm{e}^{\mathrm{i}(L/2)x}$, which is in the form of the solution assumed by Toole & Georgi (1978). The balance of the terms in the basic equations for $R \gg 1$ is given by (2.4)–(2.8), so that all the terms are important.

5. Summary and conclusions

A linear stability theory of double-diffusive horizontal intrusions in a temperature–salinity front has been formulated. The stability of the front is described by three non-dimensional parameters: a frontal stability parameter G, a stratification parameter μ and a Schmidt number ϵ. The front is found to be always unstable even if viscosity is included. However, it is found that disturbances that have a vertical scale larger than $4d$ cannot grow. When viscosity is present ($\epsilon \neq 0$), a modified frontal stability parameter R defined by G/ϵ rather than the frontal stability parameter G plays an important role in determining the stability. For a fixed value of the dimensionless horizontal gradient of salinity in the basic field, R is a monotonically increasing function of the dimensionless width of the front. When R is less than $40(1+\mu)^{5.4}$ (a narrow front), the vertical scale of the fastest-growing mode is of order d, which is the same scale as found in Ruddick & Turner's (1979) experiments. When it is larger than $2\times10^5(1+\mu)^{4.9}$ (a wide front), on the other hand, the vertical scale tends to be given by Toole & Georgi's scaling (1978), which was obtained for a front of infinite width.

The theoretical results have been compared with Ruddick & Turner's (1979) experiment. The wavelength of the fastest-growing mode obtained in the theory becomes of order d, but its precise value is somewhat smaller than the observed one. This is attributed to the effect of the nonlinearity and the crudeness of the assumption of constant eddy diffusivities. The predictions of the growth rate and the flow characteristics of the intrusions are quite reasonable, except that the model does not have the diffusive interfaces. Overall, the agreement between RT's experiment and the present theory is satisfactory, considering the crude model assumed in the theory.

I am grateful to Professor O. M. Phillips, who interested me in the present problem through his lecture at the Ocean Engineering Department, Woods Hole Oceanographic Institution. Discussions with and suggestions from Dr Barry Ruddick and Professors

George Veronis and Melvin Stern were very helpful to me. One of the referees suggested the use of a modified frontal stability parameter, which considerably reduces the dependence of the stability characteristics on the Schmidt number. Finally, I would like to thank all the staff and participants of the 1983 Geophysical Fluid Dynamics Summer Program at Woods Hole Oceanographic Institution for providing me with such a comfortable and stimulating environment for research.

Appendix A. Asymptotic wavenumber of the fastest-growing mode for large ϵ and/or small G

If σ is assumed to be proportional to $\epsilon^{-\alpha}$ or $G^{-\alpha}$ as ϵ becomes large or G becomes small, where α is a positive number, (3.1) gives

$$\frac{\sigma_n}{1+\mu} = \left[\frac{m^2}{(1+\mu)^2} - \frac{n^2\pi^2}{4}\right]\frac{G}{4\epsilon m^4}. \tag{A 1}$$

Thus the growth rate σ of the fastest-growing mode is located between $(1+\mu)[m^2/(1+\mu)^2-\pi^2]G/4\epsilon m^4$ and $(1+\mu)[m^2/(1+\mu)^2-\frac{1}{4}\pi^2]G/4\epsilon m^4$ when $m > (1+\mu)\pi$, or between 0 and $(1+\mu)[m^2/(1+\mu)^2-\frac{1}{4}\pi^2]G/4\epsilon m^4$ when $\frac{1}{2}(1+\mu)\pi < m < (1+\mu)\pi$. If we introduce $s = 4(1+\mu)^3\epsilon\sigma/G$ and $\tilde{m} = m/(1+\mu)$, (2.30) can be written as

$$\tan[\tilde{m}(1-\tilde{m}^2 s)^{\frac{1}{2}}] = -\left[\frac{1-\tilde{m}^2 s}{\tilde{m}^2 s}\right]^{\frac{1}{2}} \tag{A 2}$$

with $0 < s < (\tilde{m}^2-\frac{1}{4}\pi^2)/\tilde{m}^4$ for $\frac{1}{2}\pi < \tilde{m} < \pi$ and $(\tilde{m}^2-\pi^2)/\tilde{m}^4 < s < (\tilde{m}^2-\frac{1}{4}\pi^2)/\tilde{m}^4$ for $\tilde{m} > \pi$. Equation (A 2) can be solved numerically, and the value of $\tilde{m}$ that maximizes s is found to be 2.88, while the corresponding value of s is 0.047 19. This gives the asymptotic formula for the wavenumber of the fastest-growing mode and the corresponding growth rate σ:

$$m = 2.88(1+\mu). \tag{A 3}$$

$$\sigma = \frac{0.047\,19G}{4\epsilon(1+\mu)^3} = \frac{0.047\,19R}{4(1+\mu)^3}. \tag{A 4}$$

Appendix B. Non-hydrostatic case

In this appendix the case in which the hydrostatic approximation is not used is considered. The analytical consideration and the numerical calculations can be done in the same manner as described in §3. Therefore the only equations and figures that must be modified in this case will be described in the following. Since the smallest wavenumber of the fastest-growing mode is realized for $\mu = 0$, it may be sufficient to examine the non-hydrostatic effect for this case. In what follows, the notation $A : B$ means that the expression A should be replaced by B when the non-hydrostatic effect is considered.

(2.5): $$\frac{\partial w}{\partial t} = -\frac{\partial p}{\partial z} + g(\alpha T - \beta S) + \epsilon\kappa_e \frac{\partial^2 w}{\partial z^2},$$

(2.15): $$p'' - \frac{\mathrm{i}\tilde{g}\kappa_e m^3}{(\sigma+\kappa_e m^2)[N^2+\sigma(\sigma+\epsilon\kappa_e m^2)]} f' p' - \frac{m^2\sigma(\sigma+\epsilon\kappa_e m^2)}{N^2+\sigma(\sigma+\epsilon\kappa_e m^2)} p = 0,$$

(2.19): $$p'' - \frac{\mathrm{i}m^3 G}{(\sigma+m^2)[G+\delta^2\sigma(\sigma+\epsilon m^2)]} f' p' - \frac{m^2\sigma(\sigma+\epsilon m^2)}{[G+\delta^2\sigma(\sigma+\epsilon m^2)]} p = 0,$$

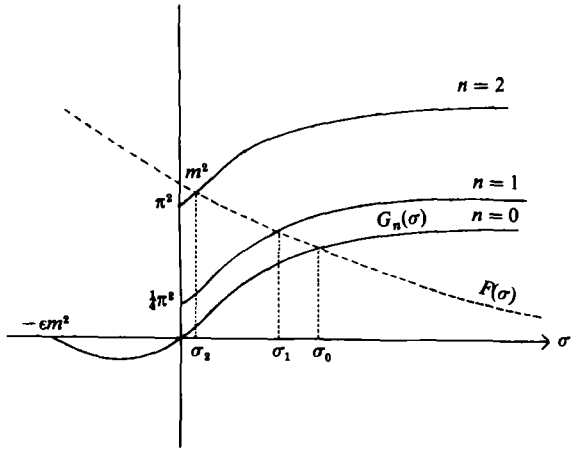

FIGURE 14. Same as figure 2, but for the non-hydrostatic case ($\delta = 1.0$) and $\mu = 0$.

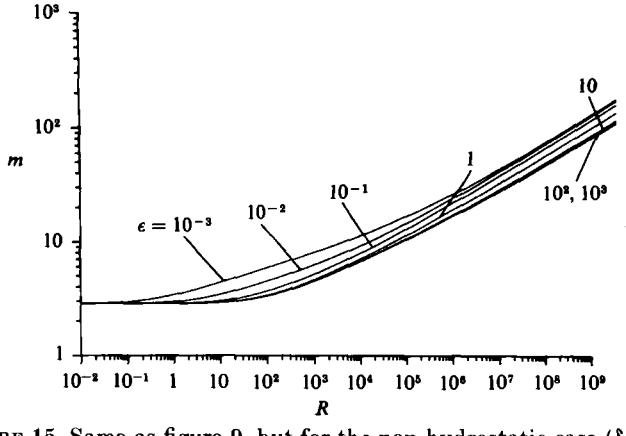

FIGURE 15. Same as figure 9, but for the non-hydrostatic case ($\delta = 1.0$).

(2.20): $$L = \frac{m^3 G}{(\sigma + m^2)[G + \delta^2\sigma(\sigma + \epsilon m^2)]},$$

(2.21): $$k = \left[\frac{m^2\sigma(\sigma + \epsilon m^2)}{G + \delta^2\sigma(\sigma + \epsilon m^2)}\right]^{\frac{1}{2}},$$

(3.1): $$\frac{m^6 G^2}{(\sigma_n + m^2)^2[G + \delta^2\sigma_n(\sigma_n + \epsilon m^2)]^2} = \frac{4\sigma_n(\sigma_n + \epsilon m)^2}{G + \delta^2\sigma_n(\sigma_n + \epsilon m^2)} + \frac{n^2\pi^2}{4}, \tag{B 1}$$

figure 2: figure 14,

(3.2): $$m^2G^2 = \begin{cases} 4\sigma_n^2 m^2(G + \delta^2\sigma_n^2) & (\epsilon = 0), \\ 4\epsilon m^4\sigma_n(G + \delta^2\epsilon m^2\sigma_n^2) & (\epsilon \neq 0), \end{cases}$$

(3.3): $$\sigma_n \to \begin{cases} \dfrac{G}{2[1 + (1 + \delta^2)^{\frac{1}{2}}]} + O(m^{-2}) & (\epsilon = 0), \\ \dfrac{R}{2[1 + (1 + \delta^2)^{\frac{1}{2}}]m^2} + O(m^{-4}) & (\epsilon \neq 0), \end{cases}$$

figure 9: figure 15,
figure 10: figure 16.

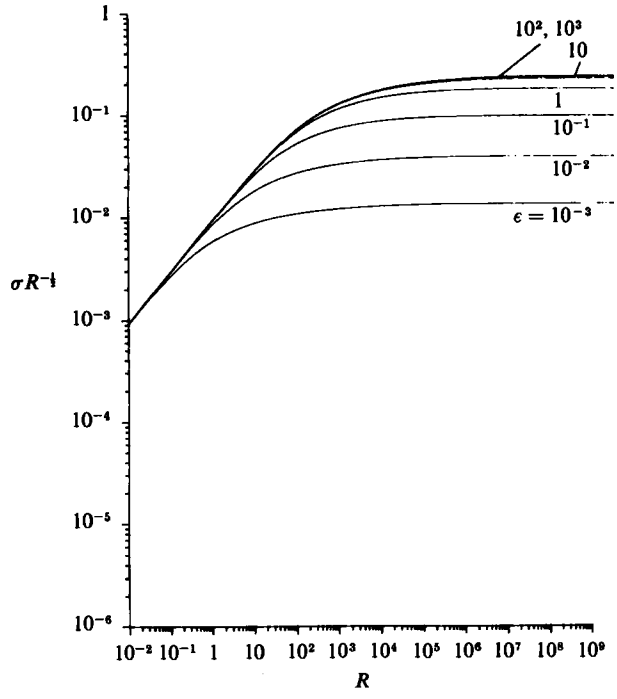

FIGURE 16. Same as figure 10, but for the non-hydrostatic case ($\delta = 1.0$).

The growth rate as a function of the wavenumber for the non-hydrostatic case is shown by the dotted lines in figures 7 and 8 for $\delta = 1.0$ and $\mu = 0$. The wavenumber and the growth rate of the fastest-growing mode for various combinations of (R, ϵ), $\delta = 1.0$ and $\mu = 0$ are shown in figures 15 and 16 respectively. It is suggested from these figures that non-hydrostatic effects are not significant for the intrusions in RT's experiment after the initial disturbances have died down.

REFERENCES

CHEN, C. F., BRIGGS, D. G. & WIRTZ, R. A. 1971 Stability of thermal convection in a salinity gradient due to lateral heating. *Intl J. Heat Mass Transfer* **14**, 57–65.

GREGG, M. C. & MCKENZIE, J. H. 1979 Thermohaline intrusions lie across isopycnals. *Nature* **280**, 310–311.

GRIFFITHS, R. & RUDDICK, B. R. 1979 Accurate fluxes across a salt–sugar finger interface deduced from direct density measurements. *J. Fluid Mech.* **99**, 85–95.

HORNE, E. P. W. 1978 Interleavings at the subsurface front in the slope water off Nova Scotia. *J. Geophys. Res.* **83**, 3659–3671.

JOYCE, T. M., ZENK, W. & TOOLE, J. M. 1978 The anatomy of the Antarctic Polar Front in the Drake Passage. *J. Geophys. Res.* **83**, 6093–6113.

MCDOUGALL, T. J. & TAYLOR, J. R. 1984 Flux measurements across a finger interface at low values of the stability ratio. *J. Mar. Res.* **42**, 1–14.

NIINO, H. & MISAWA, N. 1984 An experimental and theoretical study of barotropic instability. *J. Atmos. Sci.* **41**, 1920–1939.

RUDDICK, B. R. & TURNER, J. S. 1979 The vertical length scale of double diffusive intrusions. *Deep-Sea Res.* **26A**, 903–913.

SCHMITT, R. W. 1979 Flux measurements on salt fingers at an interface. *J. Mar. Res.* **37**, 419–436.

STERN, M. E. 1967 Lateral mixing of water masses. *Deep-Sea Res.* **14**, 747–753.

STERN, M. E. & TURNER, J. S. 1969 Salt fingers and convecting layers. *Deep-Sea Res.* **16**, 497–511.

THORPE, S. A., HUTT, P. K. & SOULSBY, R. 1969 The effects of horizontal gradients on thermohaline convection. *J. Fluid Mech.* **38**, 375–400.

TOOLE, J. M. & GEORGI, D. T. 1981 On the dynamics and effects of double-diffusively driven intrusions. *Prog. Oceanogr.* **10**, 121–145.

TURNER, J. S. 1978 Double-diffusive intrusions into a density gradient. *J. Geophys. Res.* **83**, 2887–2901.

YOSHIZAKI, M. 1982 Stability of finite-amplitude baroclinic waves in a two-layer channel flow. Part II. Moderately non-linear regime. *J. Met. Soc. Japan* **60**, 620–637.